Biosensors and Bioelectronics 47 (2013) 436–444

Contents lists available at SciVerse ScienceDirect

Biosensors and Bioelectronics

journal homepage: www.elsevier.com/locate/bios

A generic microfluidic biosensor of G protein-coupled receptor activation—monitoring cytoplasmic [Ca^{2+}] changes in human HEK293 cells

Margriet Roelse [a], Norbert C.A. de Ruijter [b], Elwin X. Vrouwe [c], Maarten A. Jongsma [a,d,*]

[a] Plant Research International, Wageningen UR, Droevendaalsesteeg 1, 6708 PB Wageningen, The Netherlands
[b] Lab. of Cell Biology, Wageningen UR, Droevendaalsesteeg 1, 6708 PB Wageningen, The Netherlands
[c] Micronit Microfluidics BV, Colosseum 15, 7521 PV Enschede, The Netherlands
[d] NanoNextNL, P.O. Box 3021, 3502 GA Utrecht, The Netherlands

ARTICLE INFO

Article history:
Received 25 February 2013
Received in revised form
22 March 2013
Accepted 26 March 2013
Available online 3 April 2013

Keywords:
G protein-coupled receptor
[Ca^{2+}] imaging
HEK293 cells
FRET
Dynamic
Microfluidic flow cell
Cameleon

ABSTRACT

Cell lines expressing recombinant G-protein coupled receptors (GPCRs) are activated by specific ligands resulting in transient [Ca^{2+}] rises that return to basal levels in 30–60 s. Yellow Cameleon 3.6 (YC3.6) is a genetically encoded calcium indicator which can be co-expressed to monitor these cytosolic [Ca^{2+}] changes in real-time using Förster (Fluorescence) resonance energy transfer (FRET). On this basis, we designed the prototype of a generic microfluidic biosensor of GPCR activation, imaging [Ca^{2+}] changes in recombinant human HEK293 cells, which express a combination of a GPCR (Neurokinin 1) and YC3.6. An internal reference for non-specifically induced [Ca^{2+}] changes were YC3.6 cells without GPCR but expressing a red fluorescent protein (mCherry) for identification. These cell lines were grown as a mixed population in a flow cell with a volume of ~50 μl and a flow cell surface of 170 mm^2. Cells were activated by brief exposures to specific and non-specific analytes using an injection valve with a flexible sample volume (tested range 5–100 μl) at a flow speed of 100 μl/min. A flow cell surface of 0.2 mm^2 with 50 cells was imaged every 2–4 s to obtain signal kinetics. The lower limit of detection was 30 pM Substance P (SP, 2 pg/50 μl), and reproducible responses to repeated injections every 3 min were obtained at 1 nM SP. This biosensor was designed for ~50 cells for statistical reasons, but at a lower limit of 1 receptor- and 1 reference-cell, specific ligand detection is still feasible.

1. Introduction

G protein-coupled receptors (GPCRs) in humans represent a family of around 800 genes which play key roles in many physiological or disease-related processes and also determine our sense of smell and taste. For this reason these receptors are favorite targets for both the pharmaceutical and food industries (Beets et al., 2011; Lappano et al., 2011; Rosenbaum et al., 2009; Saito et al., 2009; Yarmolinsky et al., 2009). Microtiter plate based high-throughput screening platforms are well established, but microfluidic technologies hold potential for miniaturization and automation that are predicted to redefine the format and application areas of GPCR screening assays (Allen and Roth, 2011; Martins et al., 2012; Wieder et al., 2005; Wu et al., 2010; Yarmush, 2009).

The most common methods of measuring GPCR activation in vivo in real-time are by recording concentration dynamics in generic secondary messengers such as [Ca^{2+}], cAMP and IP_3 using various indicator dyes (Berridge and Roderick, 2003; Paredes et al., 2008). The concentration of cytosolic [Ca^{2+}] is very low (nanomolar range) when cells are not triggered. External signals can cause the rapid release of micromolar concentrations of calcium into the cytosol from organelles like the endoplasmic reticulum (ER), mitochondria and nuclei or from extracellular sources (Yu and Hinkle, 2000). Once released into the cytosol, the [Ca^{2+}] rise is transient and levels fall back to basal levels within less than 1 min after the ligand is washed away due to uptake by the ER and mitochondria. In cell populations concentrations of cytosolic [Ca^{2+}] are directly related to the concentrations of the activating ligand, except for a subclass of GPCR receptors, which couple to Gα proteins (e.g. $G_{i/o}$, G_s, $G_{12/13}$) that, depending on the cell line, actually inhibit this response or bypass it. In those cases, overexpression of specific promiscuous Gα proteins or cAMP-gated ion channels can steer the response toward the desired [Ca^{2+}] assay (Kostenis et al., 2005). The duration of the [Ca^{2+}] transient depends among others on receptor sensitivity and ligand concentration and duration.

* Corresponding author at: Plant Research International, Wageningen UR, Droevendaalsesteeg 1, 6708 PB Wageningen, The Netherlands. Tel.: +31 317 480932
E-mail addresses: margriet.roelse@wur.nl (M. Roelse), norbert.deruijter@wur.nl (N.C.A. de Ruijter), elwin.vrouwe@micronit.com (E.X. Vrouwe), maarten.jongsma@wur.nl, maarten.jongsma@gmail.com (M.A. Jongsma).

0956-5663/$ - see front matter © 2013 Elsevier B.V. All rights reserved.
http://dx.doi.org/10.1016/j.bios.2013.03.065

The increase of [Ca^{2+}] concentration in the cytosol resulting from GPCR signaling can be measured by small molecule organic indicators like fura-red, indo-1 and many others (Paredes et al., 2008), but genetically encoded calcium indicators (GECIs), such as cameleon and GECO can also be used (McCombs and Palmer, 2008; Miyawaki et al., 1997; Palmer and Tsien, 2006; Palmer et al., 2011; Zhao et al., 2011) The choice of the calcium indicator type largely depends on the spatial and temporal resolution that is required to monitor calcium signaling processes. Current advantages of small molecule indicators are their expanded dynamic range for measuring [Ca^{2+}] concentrations and faster response kinetics. The use of GECIs, however, offers advantages in other areas. Here, we used a GECI, because it can be fused to any receptor protein of interest allowing the measurement of [Ca^{2+}] in micro-domains in its immediate vicinity. Furthermore, co-expression of GECI with receptor genes allows that only transfected cells are monitored. In case of stably transfected lines, the GECIs are immediately available for measurements and do not leak out over time, which is an important advantage when they are used in diagnostics and microfluidic biosensors. Cameleon YC3.6 is a GECI with a suitable dynamic range for measuring calcium dynamics from GPCR activation, while displaying acceptable response kinetics (Borst et al., 2008; Nagai et al., 2004). Calcium signaling from YC3.6 is based on fluorescence energy transfer (FRET) that can occur when the two fluorescent proteins of the yellow cameleon molecule; CFP and YFP are in close vicinity. These fluorescent proteins are linked together by a calmodulin domain and M13 peptide. The M13 peptide binds calcium-bound calmodulin, and thereby changes the conformation of the sensory part upon calcium binding.

Co-expression of GECI and GPCR proteins can be achieved from a polyprotein by employing a 2A polypeptide sequence between the two proteins (de Felipe et al., 2006). This has the advantage that the GECI expression level is correlated with the GPCR density on the membrane. The 2A peptide of 20 amino acids is cloned to link the coding sequences of the two recombinant proteins. During translation of the 2A part of the polyprotein the ribosomal machinery fails to create a peptide bond between two specific amino acids of the 2A peptide, but continues translation of the remaining mRNA molecule. This results in the expression of both proteins at equimolar levels (Goedhart et al., 2011; Hu et al., 2009).

Despite their predicted importance only very few studies have shown successful methods of studying [Ca^{2+}] changes in microfluidic formats (Zhang et al., 2006) and with recombinant expressed GPCRs (Feng et al., 2007; Zhao et al., 2011). These reports have neither explored the limits of detection, nor the dynamics of the cell response under different conditions. Also at a practical level, the robustness of the set-ups for automated, repeated dosage of analytes was not explored (Martins et al., 2012). In this study we developed a biosensor of GPCR activation, based on the co-expression of a GPCR and a GECI in human HEK293 cells. A new commercially available microfluidic set-up is described, which allows sequential injections of small and defined volumes of ligands at short time intervals, while maintaining a constant flow of medium across the cells contained in a resealable flow cell. As model GPCR, we used the Neurokinin 1 receptor (NK1) for this study. Upon interaction with its substrate Substance P (SP), the NK1 receptor activates the Gα subunit and effects downstream signaling by IP_3, resulting in an increase of intracellular calcium ions by release from the ER (Grady et al., 1995; Maggi, 1995; Meshki et al., 2009). Calcium responses are monitored in real-time using a confocal fluorescent microscope set-up. Reference cells monitoring endogenous activation of the cell line at the experimental conditions, thus allow determination of the specificity of activation in relation to the GPCR response. Addition of a known concentration of a fluorescent marker to the flow cell microfluidics provides a semi-quantitative real-time correlation of extracellular ligand concentrations to intracellular [Ca^{2+}] concentration changes.

2. Material and methods

2.1. DNA constructs

The NK1 receptor gene was purchased at the UMR cDNA Resource Center of the University of Missouri-Rolla, USA (cat. Nr. TACR100000). The YC3.6 gene in pCDNA3 (Invitrogen) was obtained from Roger Tsien (USA). The NK1 gene was cloned into pSNAPf (New England Biolabs) without stop codon using the *Eco*RV and *Eco*RI sites of MCS1. Oligo's of T2A (GAATTCGAGGGCAGAGGAAGTCTTCTAACATGCGGTGACGTGGAGGAGAAT**CCCGGC**CCTGGATCC=EGRGSLLTCGDVEEN**PG**P) and T2A-NC (GAATTCGAGGGCAGAGGAA GTCTTCTAACATGCGGTGACGTGGAGGAGAAT**GCCGCACCT**GGATCC=EGRGSLLTCGDVEEN**AA**P) were hybridized and cloned into pSNAPf using *Eco*RI and *Bam*HI replacing the SNAPf gene. The YC3.6 gene is cloned without start codon, but with stop codon into MCS2 using *Bam*HI and *Xho*I. Control construct mCherry-T2A-YC3.6 was cloned by PCR (FW 5′ATAT**GGCGCGCC**ATGGTGAGCAAGGGCGAGGA and RV 5′ ATAT**GAATTC**CTTGTACAGCTCGTCCATGC) from plasmid pENTRmCherry (Life Technologies Europe BV, Bleiswijk, NL), using *Asc*I and *Eco*RI restriction sites. Plasmids containing single CFP and YFP; pcDNA3-CFP (Addgene plasmid 13030) and pcDNA3-YFP (Addgene plasmid 13033) were obtained from Addgene Inc.

2.2. Cell culture and transfection

HEK293 cells (Invitrogen, 11631-017) were grown as a monolayer in cell culture medium (Dulbecco's Modified Eagle Medium (DMEM) containing 1 × MEM non-essential Amino Acids, 1 × Penicillin–Streptomycin (Invitrogen, 15140-122) and 10% Fetal bovine serum FBS (Invitrogen, 26140)). Cells were transfected with expression vectors pNK1-T2A-YC3.6, pNK1-T2ANC-YC3.6 and mCherry-T2A-YC3.6 using Effectene transfection reagent (Qiagen 301425). Selection with Geneticin at 600 μg/ml (Invitrogen) was started 24 h after transfection and maintained for several weeks until stable expressing cell cultures were obtained. From a stable expressing cell culture a clonal line with intermediate YC3.6 expression, visually identified based on mean fluorescence intensity, was selected.

2.3. Western blotting

Cells were harvested at about 80% confluency, and resuspended in 1/5 volume RIPA buffer (Sigma-Aldrich, R0278) containing complete protease inhibitor cocktail (Roche 11 697 498 001). Samples were denatured in reducing SDS-PAGE sample buffer, separated on 12.5% SDS-PAGE gel and transferred to nitrocellulose membrane by Western blotting. The GFP protein and spectral variants CFP and YFP were detected with mouse anti-GFP (Roche 11 814 460 001) 1:5000 diluted in blocking buffer and sheep anti-mouse HRP (Jackson Immuno 515-035-062) 1:5000 diluted in blocking buffer.

2.4. Flow cell assembly and microfluidics

All imaging was performed in resealable borosilicate glass flow cells (Micronit Microfluidics B.V., Enschede, The Netherlands). Temperatures were maintained at 22 °C (RT) unless otherwise noted. Recombinant HEK293 cells were seeded on a disposable 15 × 45 mm^2 borosilicate coverslide of standard (1.5 #) 175 μm thickness, coated with 100 μg/ml poly-L-Lysine (Sigma P6282) at a density of ~3×10^5 cells/ml. The slides were incubated overnight in a sterile petridish in a CO_2 incubator at 37 °C. Next, a re-usable borosilicate glass slide of 15 × 45 mm^2 and 1.1 mm thickness with a central 0.3 mm high gasket of 5 × 43 mm (defining a flow cell

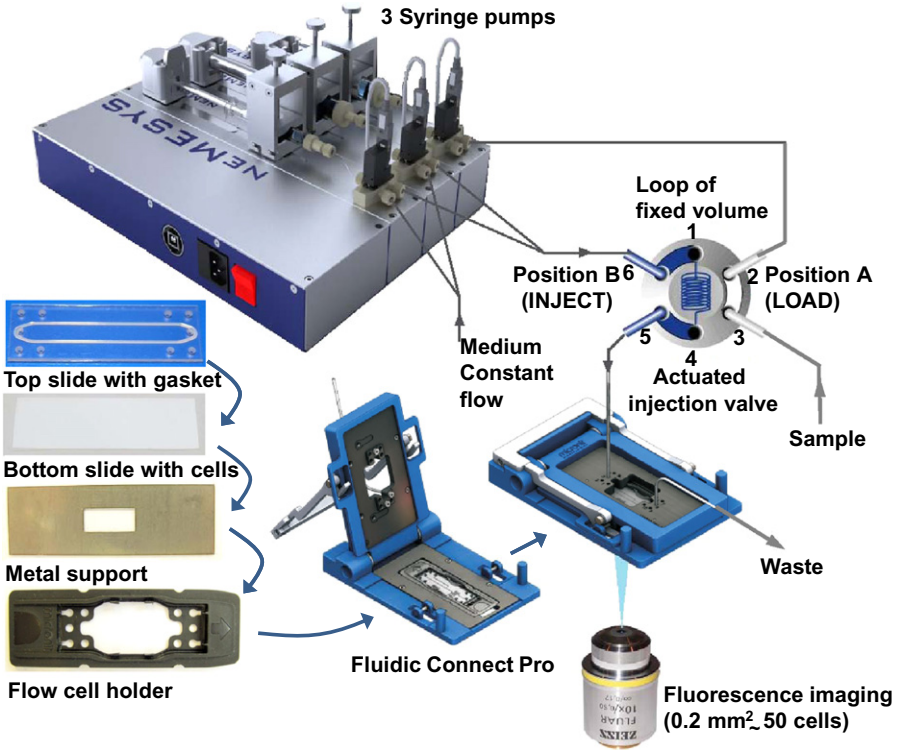

Fig. 1. Diagram of the microfluidic biosensor set-up. The microfluidic flow cell of 50 μl is assembled in the blue Fluidic Connect Pro flow cell holder by mounting the indicated parts. Closing the holder connects the capillaries for dosing media and samples. Two syringe pumps maintain a constant flow of cell media by alternated uptake and dosing into the flow cell through ports 5 and 6 of the injection valve. Ports 2 and 3 are used to fill and empty/wash an injection loop using the third syringe. Switching the injection valve from LOAD to INJECT assures that samples of various volumes depending on the loop size are injected into the flow cell and vice versa that the loop can be reloaded. Fluorescence changes in the cell monolayer are imaged.

inner surface area of ~170 mm^2) was placed over the coverslide with cells to create the flow cell with cells inside (Fig. 1, Micronit Microfluidics BV, Enschede, The Netherlands). Two fluidic ports in the slide, 40 mm apart, served for microfluidic connections. The assembled flow cell was placed on a metal supporting plate of 15×45 mm^2 with opening of 5×11 mm^2 at the bottom to prevent deformation of the thin lower cover slide. The slides were sealed together in a Fluidic Connect Pro flow cell holder (Micronit Microfluidics B.V., Enschede, the Netherlands), which allowed immediate fluidic connection of the flow cell to a set of syringe pumps (Nemesis, Cetoni GmbH) that controlled a constant flow of cell culture medium (100 μl/min; port 5 and 6 in Fig. 1). Injection of samples loaded in a sample loop was performed using an injection valve (Upchurch, V-451); 5–100 μl loop volume between port 1 and 4 for injection and port 2 and 3 for loading and rinsing of the sample loop.

2.5. FRET imaging using confocal laser scanning microscopy

Imaging of cameleon YC3.6 was performed with a Zeiss LSM 510-META 18 confocal laser scanning microscope on an Axiovert 200M equipped with a 20× 0.5 NA Plan-Neofluar DIC objective using the 458 nm line from a 30 mW Ar laser. With a series of detectors in the META channel a stack of 10.7 nm spectrally resolved images were recorded, called Lambda Stacks (465–610 nm). This allowed pixel-by-pixel collection and separation of the simultaneously recorded CFP and YFP emissions, based on reference spectra taken at identical imaging settings. Imaging was done at the cellular mid-plane with wide pinholes of 2.91 AU (Airy Unit) corresponding with a 10 μm thick optical slice. The emission fingerprint-based CFP and YFP intensities of regions of interest were plotted in 2 s interval time series and their ratiometric FRET signals analyzed. For this, HEK293 cells were transfected with reference plasmids pcDNA-CFP or pcDNA-YFP. Both cultures were used to record reference lambda stacks required for spectral unmixing at 458 nm excitation. An additional reference emission spectrum for fluorescein was recorded at 458 nm with imaging settings as used during experiments, to allow spectral unmixing in the presence of this internal dilution standard, Fluorescein concentrations were below saturating concentrations in all experiments to avoid errors in spectral unmixing. Confocal imaging of TAMRA-labeled Substance P (SP^{TAMRA}, Anaspec cat nr. 61202) was done with HeNe laser of 543 nm and pinhole at 1 AU to obtain the maximal z-resolution.

3. Results and discussion

3.1. DNA constructs for biosensor cell lines

To enable a GECI-based system, genetic constructs were developed to co-express a model G-protein coupled receptor, Neurokinin 1 (NK1), and the GECI Cameleon YC3.6 from a single transcript, but as separate proteins (Fig. 2A). The two genes were separated by either the native T2A peptide linker, resulting in two translation products, or the mutated non-cleavable version T2ANC, resulting in a single multiprotein (de Felipe et al., 2006; Goedhart et al., 2011; Hu et al., 2009; Szymczak et al., 2004). The aim of using a 2A construct was to obtain correlated expression levels of the receptor unit and the genetically encoded calcium indicator. The aim of using the T2ANC construct was to allow the visualization of the receptor on the plasma membrane and creating a single molecule capable of both extracellular sensing and monitoring of intracellular [Ca^{2+}] proximal to the plasma membrane.

The HEK293 cell line used to express these DNA constructs also carries native receptors on its surface which can also generate

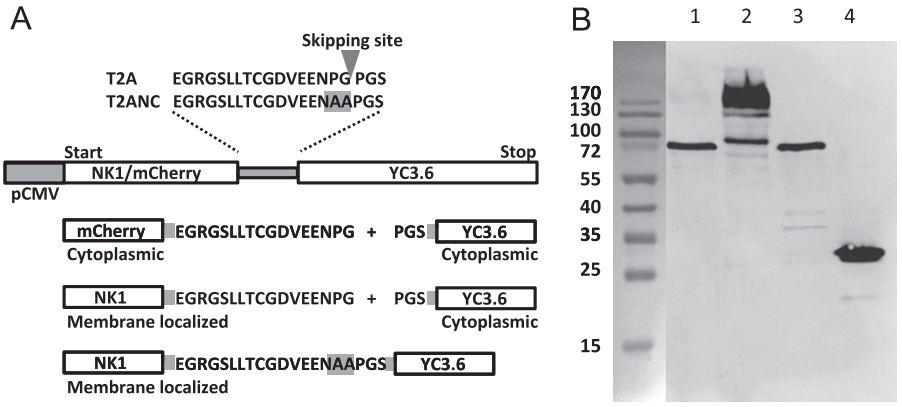

Fig. 2. DNA and protein constructs to generate green GPCR and red reference cells. **A**: Top bar the DNA construct used for the transformation of HEK293 cells with either a GPCR target receptor (NK1) as biosensor or a red protein (mCherry) to tag reference cells. Lower three bars represent the expressed proteins. **B**: Western blot identifying YC3.6 containing polypeptides. Protein extracts of HEK293 cell lines expressing various constructs were separated by 12.5% SDS-PAGE, blotted to nitrocellulose membrane, and detected with anti-GFP antibody. The molecular weight of GFP is 27 kDa, YC3.6 is 72 kDa and NK1 is 45 kDa. Lane 1: pNK1-T2A-YC3.6; Lane 2: pNK1-T2ANC-YC3.6; Lane 3: YC3.6; Lane 4: GFP.

$[Ca^{2+}]$ changes signals which may interfere with the signal from the NK1 receptor. To distinguish specific responses induced by the targeted receptor from non-specific cell responses, it is necessary, to measure in parallel reference cells, which do not ectopically express any recombinant $[Ca^{2+}]$ changes inducing receptor, but do possess the fluorescent calcium reporter YC3.6. To recognize such cells we replaced the gene for the receptor with the one encoding red fluorescent protein, mCherry (Fig. 2A).

3.2. Subcellular localization of the membrane receptor and calcium-indicator protein

For all constructs, stable HEK293 clonal cell lines were made by selecting recombinant cell lines with stable integrated plasmid DNA and sub-culturing into a clonal line. The T2A and T2ANC peptides determine whether the protein fusions are expressed as one or two separate proteins. To verify the presence of the expected translation products and the efficiency of the T2A-induced ribosome skipping, protein extracts were analysed by Western blot using an antibody against GFP and spectral variants CFP and YFP (Fig. 2B). A YC3.6 expressing cell line (without the mCherry protein or receptor) showed a 72 kDa band, which corresponds with the expected size of the cameleon protein. The cell line expressing the NK1 receptor and YC3.6 linked by the T2A polyprotein linker showed a single band with a size of 72 kDa as well, which indicates that the first protein, the NK1 receptor, is fully cleaved from YC3.6 and that T2A-mediated ribosome skipping is very efficient. The cell line expressing the NK1 receptor and YC3.6 linked by the non-cleavable T2ANC peptide was expected to yield a fusion protein of 117 kDa. Next to two minor bands of 100 kDa and 130 kDa most signal, however, is of higher molecular weight. Since cameleon is fused to a membrane protein, which is known to resist complete SDS denaturation, it probably represents poorly dissolved fusion protein.

To demonstrate the functional plasma membrane localization of the NK1 receptor, SP^{TAMRA} was used (Bennett and Simmons, 2001). Confocal imaging showed that SP^{TAMRA} is bound to the plasma membrane of cells expressing recombinant NK1 receptor from both T2A and T2ANC constructs (Fig. 3A and D). SP^{TAMRA} did not bind to the membrane of WT cells, since HEK293 cells do not endogenously express the NK1 receptor (results not shown). Differences between the two constructs were clearly visible from the localization of the cameleon protein (Fig. 3B and E). The T2A construct releases the cameleon protein which accumulates in the cytoplasm. The T2ANC construct on the other hand fuses the cameleon protein to the cytoplasmic C-terminus of the membrane bound NK1 receptor, and as a result membrane co-localization of YC3.6 and SP^{TAMRA} on the membrane is visible in Fig. 3F, but not in Fig. 3C.

Previous studies (Meshki et al., 2009) have shown that binding of SP to NK1 results in activation of the downstream signaling pathway leading to a temporal rise in cytoplasmic calcium ion concentrations (Section 3.5) and, also, irregular bulges of the plasma membrane known as membrane blebbing as clearly visible for both constructs in Fig. 3.

3.3. Design of a resealable microfluidic flow cell

We aimed to develop a biosensor capable of specifically measuring GPCR-activating analytes in a series of samples using fluorescence imaging. For best optical and chemical properties and easy handling, a resealable flow cell was designed composed of two borosilicate glass slides separated by a gasket of fluorinated elastomer which included a microfluidic inlet and outlet (Fig. 1). The slides were sealed together in a Fluidic Connect Pro flow cell holder (Micronit), which allowed immediate fluidic connection to a set of 3 syringe pumps that provided a constant flow of cell culture medium, and, using an injection valve (5–100 μl loop volume), seamless introduction of samples. Cells remained adherent to the polylysine modified surface at flow speeds below 400 μl/min. The flow cell dimensions were 170 $mm^2 \times 0.3$ mm, but in principal the surface could be 800× smaller as we monitored an area of only ~0.2 mm^2 containing ~50 cells.

3.4. Image acquisition and analysis

After excitation with 458 nm a confocal laser microscope collected image emission spectra every 2 s for 512 × 512 pixels. This image series was automatically analyzed by spectral unmixing on a pixel-by-pixel base to provide a value of the change in FRET (YFP/CFP ratio) resulting from the cytosolic calcium transients. For image processing we applied a custom made plugin named PRI-FRET on ImageJ (v1.46). This plugin can set lower and upper threshold values on the YFP and CFP images to remove background noise and saturated intensity pixels, and subsequently ratio and average relative intensities of all remaining dynamic YFP and CFP pixels over time. All ratio averages were subsequently normalized by subtraction of the averages of those ratios obtained before injection.

Without an internal reference to remove non-specific responses this biosensor would be a general sensor of $[Ca^{2+}]$ changes inducing analytes, but not of a particular GPCR. As we

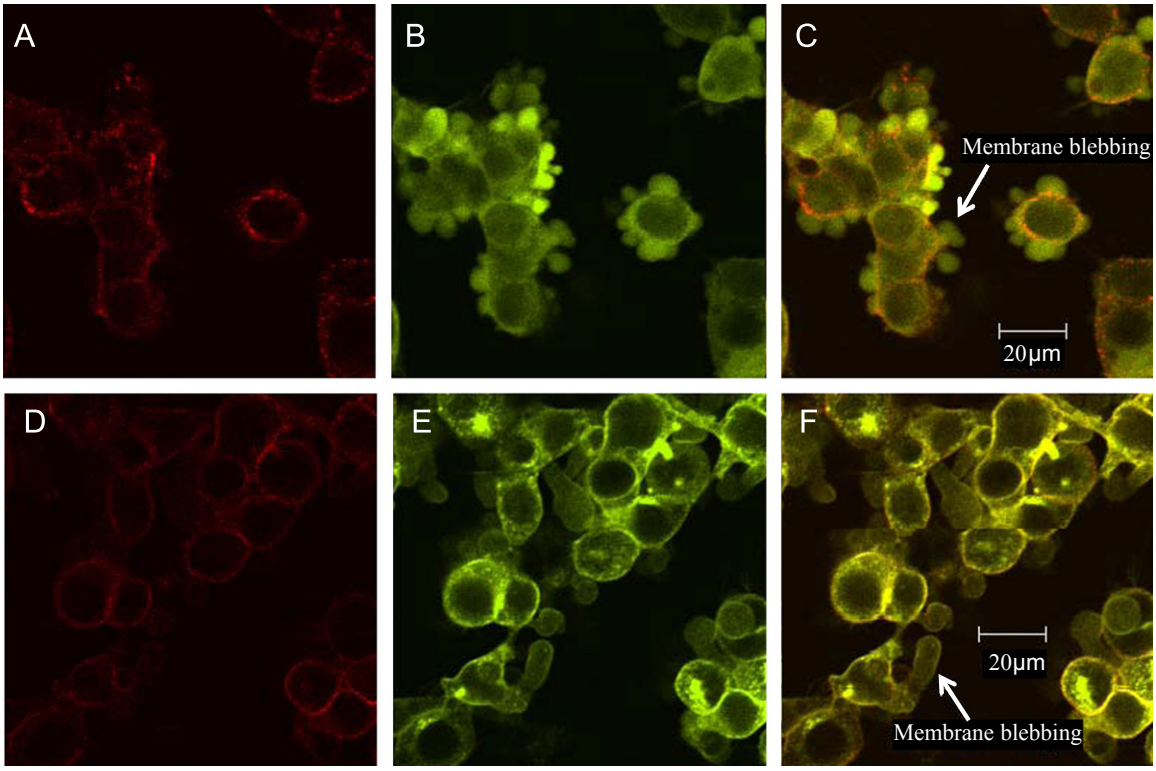

Fig. 3. Confocal images of HEK293 cells expressing cytoplasmic cameleon from NK1-T2A-YC3.6 (**A**, **B** and **C**) and membrane associated cameleon from NK1-T2ANC-YC3.6 (**D**, **E** and **F**) shortly after adding 50 nM SP^{TAMRA}. Pictures **A** and **D** show SP^{TAMRA} localized on the cell membrane by excitation at 543 nm. **B** and **E** show cameleon YC3.6 localization by direct excitation of YFP at 514 nm. **B** shows cytoplasmic localization of YC3.6 and **E** shows localization of YC3.6 on the membrane and in intracellular compartments like the ER. **C** and **F** are overlay images of **A**+**B** and **D**+**E** respectively. SP-induced membrane blebbing is indicated.

only observe statically within a single flow channel, we introduced a method for automatic detection and subtraction of non-specific signals by mixing the GPCR cells 3:1 with red colored reference cells expressing the red fluorescent protein mCherry instead of the receptor (Fig. 2A). We made use of the fact that mCherry has an excitation optimum of 543 nm, which does not excite the YFP or CFP proteins of YC3.6. Processing of images with a mix of receptor and reference cells was done by input of a reference cell image. Before or after the FRET time series a single mCherry image was made to determine which cameleon pixels were derived from reference cells. The software then generated separate normalized ratio curves for the receptor and reference cells.

3.5. Specificity

To test the GPCR biosensor specificity Fig. 4A and B shows the results after injection of an NK1-specific ligand versus a non-specific ionophore for calcium ions across membranes. Plotted are the signal averages from single cells and ~50 cells in the same view. The receptor specific ligand SP (10 nM) increased FRET signals only in the receptor cells and not in mCherry cells (Fig. 4A). Injection of 2 µM ionomycin (Free Acid, *Streptomyces conglobatus*, Calbiochem) resulted in responses in both NK1 receptor and mCherry reference cells. Thus this design allows that non-specific signals from mCherry cells can be deducted automatically from signals obtained from the GPCR cell fraction to ensure that the recorded responses are GPCR-specific.

3.6. Sensitivity range

To determine the lower and upper sensitivity range of the NK1 receptor, response curves were made for both the T2A and T2ANC receptor constructs of NK1. Injections of 50 µl SP at concentrations ranging from 1 pM to 100 nM at a flow speed of 100 µl/min were performed to measure the activation of the NK1 receptor. At concentrations above 1 nM SP a fresh slide was used for each measurement to avoid effects of receptor saturation from previous runs. Fig. 4C and D shows the correlation of peak area and height of transient FRET ratio curves with SP concentration. For the NK1-T2A-YC3.6 clone the optimal SP concentration range (linear part of the S-curve) based on measured peak heights (Fig. 4D) was 25–2500 pM, whereas for peak area (Fig. 4C) it ranged from 100–5000 pM. For the NK1-T2A-NC-YC3.6 clone the optimal SP concentration range based on peak height (Fig. 4D) was 100–2500 pM and for peak area (Fig. 4C) it ranged from 250–25000 pM. In both dose response curves the T2ANC cell line reached higher maximum values. The cell lines were clonal lines, which meant that all cells express approximately the same number of receptor molecules on the membrane. The response differences may be explained by the possibility that clone NK1-T2ANC-YC3.6 has more or stronger expressed copies of the NK1 receptor gene, and, therefore, a higher density of receptors available on the surface compared to the NK1-T2A-YC3.6 clone. Higher densities of receptors lead to stronger activation of the transient [Ca^{2+}] changes and higher maximum values in the dose response curve.

3.7. Measurement throughput and regeneration time

Earlier studies describe that after activation, the NK1 receptor internalizes in endosomes followed by receptor dissociation from the ligand and receptor recycling back to the membrane, while the ligand is degraded internally (Grady et al., 1995). As a result there is a transient drop in the number of available receptor sites. This phenomenon is especially relevant for a biosensor application in which cells are repeatedly exposed to potentially

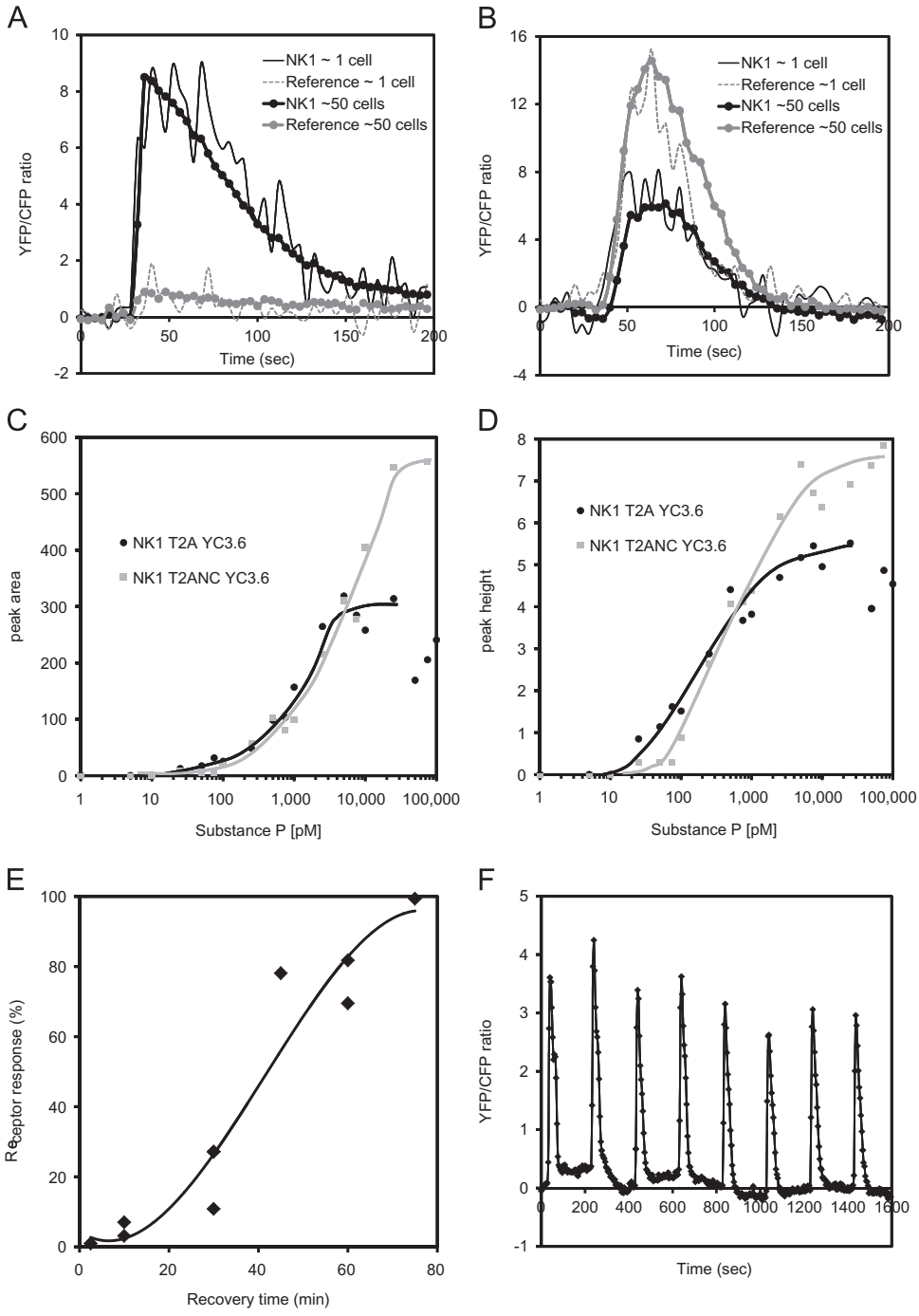

Fig. 4. NK1-biosensor evaluation in terms of specificity, sensitivity, dose-response, time-to-recovery, and re-usability. Cameleon FRET ratioing monitors $[Ca^{2+}]$ changes in the mixed NK1 and mCherry reference cells. Response profiles of ca 50 mixed cells were imaged every 2 s in one field of view (0.2 mm^2) while injecting (**A)** 10 nM SP and (**B**) 2 μM ionomycin. Red mCherry cell pixels were graphically separated from the green NK1 cell pixels. Injection of the NK1-specific ligand SP yielded only a $[Ca^{2+}]$ changes in NK1 expressing cell(s), and injection of the non-specific ionophore ionomycin yielded $[Ca^{2+}]$ changes in both NK1 and reference cells. The signals for both 50 and single cells are given. Dose-response curves based the integrated peak area (**C**) and the maximum peak height (**D**) are plotted against the ligand concentration. In **E** the recovery time of the NK1 receptor response after a saturating injection of 50 nM SP is shown. In **F** the response of NK1 cells to injections repeated every 200 s with lower 1nM concentrations of SP is shown. Images were taken every 4 s. All experiments A–F were performed at a flow rate of 100 μl/min and with 50 μl sample.

high concentrations of activating ligands which would saturate and remove available receptor sites from the membrane.

In Fig. 4E we show, that, while maintaining cells at RT and 100 μl/min continuous flow of fresh cell culture medium, full recovery of the FRET signal, after exposing the receptor to a saturating dose of 50 nM SP, is a gradual process taking around 80 min to complete. In biosensor measurements knowledge of this recovery curve helps to interpret the reliability of subsequent measurements after the response has passed a certain threshold value.

To demonstrate the throughput of the biosensor to yield accurate responses to repeated injections of 1 nM SP, an experiment was done repeating 8 injections every 200 s using the NK1-T2A-YC3.6 cell line (Fig. 4F). A slight fluctuation in peak height was observed, probably due to fact that data points are 4 s apart, thus missing the maximum peak height between two subsequent

scans. A larger time interval between data points (4 s) was chosen to prevent photo bleaching of the YC3.6 fluorophore during continuous measurements for 30 min. The limited but apparent signal reduction of around 10% across the 8 measurements may reflect a reduction in receptor density due to the repeated activations at that concentration and frequency.

3.8. Relationship of injected sample volume to flow cell volume

Our test samples were injected via fused silica capillaries of 0.15 mm inner diameter (0.018 mm^2) and released into a flow cell of cross section 0.3 mm height × 4 mm width (1.2 mm^2). This 68-fold expansion in cross-section slows the linear flow speed, and increases the surface area over which diffusion can occur of sample analyte with media ahead and behind it. For the standard flow cell of 50 μl volume we determined the peak shapes of both the analyte concentrations and the biosensor responses after injecting 5, 50 and 100 μl of 1 nM SP at a continuous flow of 100 μl/min. The relative concentrations of analyte contacting the cells in the microscope field of view, were determined by mixing SP samples with an inert fluorescent dye as internal standard (1 μM fluorescein). By taking injection volumes 2 × larger and 10 × smaller than the flow cell volume, we were able to characterize the changes in the shape of the sample concentration profile due to increased diffusion and laminar flow effects. Fig. 5 shows the profiles of the sample concentration and FRET ratio response after injection of 100 μl SP (Fig. 5A), 50 μl SP (Fig. 5B) or 5 μl SP (Fig. 5C). Table 1 summarizes the results of Fig. 5 by giving the deviation from the expected value if there would be no diffusion or other dispersive effects. When no dispersive effects would take place, the fluorescein signal from the 5 μl loop would be expected to have the same peak height as the larger injected volumes with the same sample concentration, a duration of 3 s (FWHM) and a peak area proportional to the injected quantity. Peak height, however, was 72% lower than the injected concentration value, and peak width over 4 times broader due to diffusion. Peak area was 128% the expected value, possibly due to slower speeds of the compound close to the flow cell surface where the cells are and measurements are taken. The results show that sample diffusion has pronounced effects on sample concentration when the sample volume is much smaller (10 ×) than the flow cell volume. Also the FRET ratio response signals deviated from the expected values. Peak height was 60% lower than the expected value in correspondence with the 72% lower sample concentration. Peak width, when including the shoulder peak, was shorter than sample exposure time at long exposures of 60 s (Fig. 5A), the same at sample exposures of 30 s (Fig. 5B), and longer at sample exposures of around 13 s (Fig. 5C). This shows how these responses follow their own internal dynamics after the initial trigger. This is also visible from the two longer exposure times, which show a peak response plus an additional shoulder, which is the result of calcium oscillations (Berridge et al., 2003). The longer the receptor is exposed to the ligand, the more and the longer these oscillations occur. These peak shoulders are not very informative and the larger volumes passed through the sensor are potentially wasteful. We conclude, therefore, that the optimal sample volumes for GPCR-based cellular biosensors are equal to the volume of the biosensor flow cell and apply flow rates that allow the entire sample to be passed in less than 30 s.

Table 1
Effects of sample volume in relation to flow cell volume (50 μl) on the sample concentration (fluorescein) and FRET ratio response characteristics[a].

	Injected volume (μl)	Fluorescein characteristics[a]	Deviation from the expected value (%) [a]	FRET response characteristics[a]	Deviation from the expected value (%)[a]
Peak height	100	69 FU	0	9.9 RU	0
	50	68 FU	−2	9.6 RU	−3
	5	19 FU	−72	3.9 RU	−60
FWHM[b]	100	64 s	+6	21.5 s[c]	n.d.[d]
	50	32 s	+6	22.0 s	n.d.
	5	13 s	+332	10.5 s	n.d.
Peak area[e]	100	4388[e]	+6	356[e]	n.d.[d]
	50	2280	+10	236	n.d.
	5	282	+36	47	n.d.

[a] Substance P (1 nM) mixed with 1 μM fluorescein as internal standard was injected into a flow cell of 50 μl in volumes of 100, 50 or 5 μl. The effect of substrate dilution is quantified relative to 100 μl injected in the 50 μl flow cell.
[b] Full Width at Half Maximum (FWHM) measured in seconds.
[c] The main calcium response peak, not including the right shoulder.
[d] The deviation from the expected value for FRET signal areas was not determined since longer exposure times influence peak areas in a non-linear manner.
[e] The peak area (FU or RU × s) includes the peak shoulder.

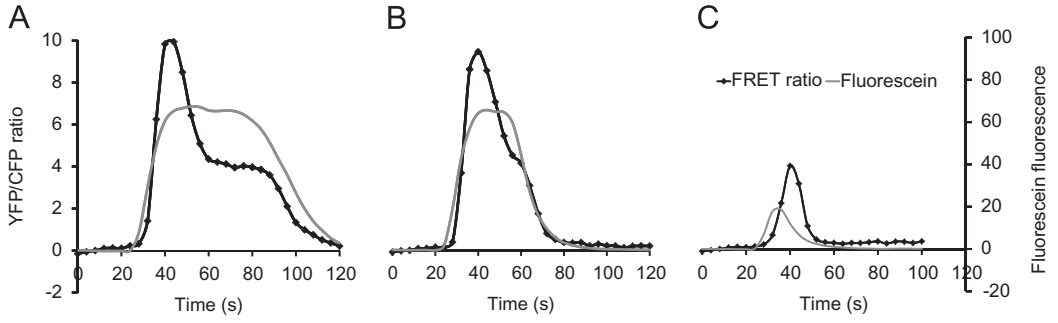

Fig. 5. Activation of the NK1 receptor by different volumes of 1 nM SP using a fluorescent marker as internal standard of the ligand concentration. Injections were done of 100 μl (**A**), 50 μl (**B**), and 5 μl (**C**) of 1nM SP into a 50 μl flow cell at a constant flow rate of 100 μl/min. The YFP/CFP ratio is plotted on the left-axis axis and the fluorescein intensity on the right-axis. Fluorescein intensity (1 μM) is measured in the background. Measurements were taken every 4 s.

4. Conclusions

The presented NK1 GPCR biosensor provides proof of principle for GPCR biosensors in general as systems with large potential for highly sensitive, flexible and quantitative microfluidic sensing devices. Unlocking the potential of utilizing the 800 human members of the GPCR gene family (and genes of other organisms) for a broad array of biosensing needs in the medical, pharmaceutical, environmental, food and cosmetic domains promises to be an exciting area of research and development. The unique components of this GPCR biosensor device provide important potential advantages over other available detection systems.

1. Cameleon—Cameleon YC3.6 is a genetically encoded calcium indicator which allows immediate measurement of cytoplasmic calcium ions concentrations, independent of indicator concentration, due to ratiometric imaging. Other systems require loading of small molecule indicators, that might get sequestered or leak out over time compromising measurement accuracy. The use of this GECI, furthermore reduces costs of chemicals and time, and improves reproducibility of measurements.
2. T2A for correlated concentrations of receptor and calcium indicator—The use of T2A or T2ANC allows a direct assessment of the receptor concentration and localization in any evaluated cell. Low expression of cameleon will be directly correlated to low expression of the receptor. This aids in the selection of the desired expression levels in clonal cell lines and provides an internal check that the receptor is expressed.
3. High content imaging—The flow cell is embedded in a chip holder, which provides a microscope viewing window, that currently allows the use of microscope objectives for detailed imaging with 20× objectives. Other designs of the current commercially available chipholder could allow spatial access of objectives with shorter working distances and higher numerical apertures to obtain images with further increased optical resolution and thus provide information about subcellular processes.
4. Sensitivity—The sensitivity of ligand detection will typically depend on the EC_{50} for the chosen receptors. In our example with NK1 and SP we could detect ca. 30 pM SP in 50 μl of sample corresponding to 2 pg of analyte. However, the system operates on sample loop injections that are optimal when they approach the flow cell volume. The commercial flow cell we used was ~50 μl with a surface area of 170 mm^2. Large reductions in flow cell volume are possible in the current design as the volume depends on the circumference of the gasket which is 850 times larger now than the monitored area of 0.2 mm^2.
5. In- or at-line measurements—The procedure of injecting samples from an injection loop into the biosensor device can be easily automated and is potentially suitable for in- or at-line measurements. We estimate that a cell based biosensor needs to be replaced every 8 h and is potentially capable of 100 measurements. The time limit of safe use will need to be experimentally verified, however, and is based on potential uncontrolled microbial infections that could start to affect cell behavior at some point. Infections can be controlled by use of antibiotics and filter sterilizing samples.
6. Data analysis—Images were processed based on an ImageJ plugin which can be automated to provide online digital graphic outputs of activities in samples.
7. Low cost detection—The system was operated on an advanced Zeiss confocal microscope using spectral unmixing. However, a normal fluorescence microscope could be used as well since YFP and CFP measurements are well possible using excitation and emission filters and even CFP measurements alone could provide a reliable output (although CFP concentration dependent). Furthermore, as signal intensity is more important for biosensors than localization confocality is not needed to measure signaling events.

The system also carries certain potential disadvantages:

1. Throughput—Even though the frequency of measurements could be raised to once every 3 min, these are sequential, and there are issues of fluorescence bleaching and receptor internalization, which at high imaging frequencies and high doses affect subsequent measurements. A possible solution to this problem would be to use the current flow cell principle to design highly parallel flow cells which can be addressed sequentially and/or in parallel at optimal frequencies to ensure reliability and to improve throughput (Park et al., 2010).
2. Handling and assembly must be done by skilled laboratory personnel—like maintaining cell cultures and operating a fluidic system and microscope. This is also true of microtiter plate based cell assays, but could be simplified if dedicated instruments will be developed.
3. Transcriptional fusions based on the T2A-peptide can also be a disadvantage—Some receptors do not allow high expression in cell lines. Selecting low expressors will then also reduce the signal intensity from cameleon. In some cases these two proteins may therefore better be uncoupled. A stable cell line with high expression of cameleon could be used for transfection of receptor proteins using a different selectable marker, thus avoiding this potential issue.
4. In a situation that a sample contains mixed compounds which trigger cumulative specific and non-specific responses the net difference between the GPCR and reference cell line responses may still contain information of the specific response. The visibility of this difference will however depend on the relative induced signal strength.

Acknowledgments

We thank Gerrit Polder from WUR-Biometris for designing Image J plugin PRI-FRET, Jan-Willem Borst from WUR Biochemistry for getting us started on FRET measurements of cameleon, Doug Golenbock, principal investigator, who submitted pcDNA3-CFP and pcDNA3-YFP to the Addgene plasmid bank, and Harrie Verhoeven and Joachim Goedhart for critically reading the manuscript. Financial support was obtained from Nano4Vitality program 2008-I, and from NanoNextNL, a micro- and nanotechnology consortium of the Government of the Netherlands and 130 partners.

References

Allen, J.A., Roth, B.L., 2011. Annual Review of Pharmacology and Toxicology 51, 117–144.
Beets, I.L.M., Janssen, T., Verleyen, P., 2011. In: Merighi, A. (Ed.), Neuropeptides: Methods and Protocols, Methods in Molecular Biology. Springer Science.
Bennett, V.J., Simmons, M.A., 2001. BMC Chemical Biology 1 (1), 1.
Berridge, M.J., Bootman, M.D., Roderick, L.H., 2003. Nature reviews 4, 517–529.
Borst, J.W., Laptenok, S.P., Westphal, A.H., Kuhnemuth, R., Hornen, H., Visser, N.V., Kalinin, S., Aker, J., van Hoek, A., Seidel, C.A., Visser, A.J., 2008. Biophysical Journal 95 (11), 5399–5411.
de Felipe, P., Luke, G.A., Hughes, L.E., Gani, D., Halpin, C., Ryan, M.D., 2006. Trends in Biotechnology 24 (2), 68–75.
Feng, X., Castracane, J., Tokranova, N., Gracias, A., Lnenicka, G., Szaro, B.G., 2007. Biosensors and Bioelectronics 22, 3230–3237.
Goedhart, J., Van, W.L., Adjobo-Hermans, M.J.W., Elzenaar, I., Hink, M.A., Gadella, T. W.J., 2011. PLos ONE 6 (11), 1–7.
Grady, E.F., Garland, A.M., Gamp, P.D., Lovett, M., Payan, D.G., Bunnett, N.W., 1995. Molecular Biology of the Cell 6 (5), 509–524.
Hu, T., Fu, Q., Chen, P., Zhang, K., Guo, D., 2009. Biotechnology Letters 31 (3), 353–359.

Kostenis, E., Waelbroeck, M., Milligan, G., 2005. Trends in Pharmacological Sciences 26 (11), 595–602.
Lappano, R., Maggiolini, M., 2011. Nature Reviews Drug Discovery 10, 47–60.
Maggi, C.A., 1995. General Pharmacology 26 (5), 911–944.
Martins, S.A., Trabuco, J.R., Monteiro, G.A., Chu, V., Conde, J.P., Prazeres, D.M., 2012. Trends in Biotechnology 989, 1–9.
McCombs, J.E., Palmer, A.E., 2008. Methods 46 (3), 152–159.
Meshki, J., Douglas, S.D., Lai, J.P., Schwartz, L., Kilpatrick, L.E., Tuluc, F., 2009. Journal of Biological Chemistry 284 (14), 9280–9289.
Miyawaki, A., Llopis, J., Heim, R., McCaffery, J.M., Adams, J.A., Ikura, M., Tsien, R.Y., 1997. Nature 388 (6645), 882–887.
Nagai, T., Yamada, S., Tominaga, T., Ichikawa, M., Miyawaki, A., 2004. Proceedings of the National Academy Sciences USA 101 (29), 10554–10559.
Palmer, A.E., Tsien, R.Y., 2006. Nature Protocols 1 (3), 1057–1065.
Palmer, A.E., Qin, Y., Park, J.G., McCombs, J.E., 2011. Trends in Biotechnology 29 (3), 144–152.
Paredes, R.M., Etzler, J.C., Watts, L.T., Zheng, W., Leichleiter, J.D., 2008. Elsevier methods 46, 143–151.
Park, E.S., Brown, A.C., DiFeo, M.A., Barker, T.H., Lu, H., 2010. Lab on a Chip 10 (5), 571–580.
Rosenbaum, D.M.E.A., 2009. Nature 459, 356–363.
Saito, H., Chi, Q.Y., Zhuang, H.Y., Matsunami, H., Mainland, J.D., 2009. science signaling 2, 60.
Szymczak, A.L., Workman, C.J., Wang, Y., Vignali, K.M., Dilioglou, S., Vanin, E.F., Vignali, D.A., 2004. Nature Biotechnology 22 (5), 589–594.
Wieder, K.J., King, K.R., Thompson, D.M., Zia, C., Yarmush, M.L., Jayaraman, A., 2005. Biomedical microdevices 7 (3), 213–222.
Wu, M.H., Huang, S.B., Lee, G.B., 2010. Lab on a Chip 10, 939–956.
Yarmolinsky, D.A., Zuker, C.S., Ryba, N.J.P., 2009. Cell 139 (2), 234–244.
Yarmush, M.L.A., King, K.R., 2009. Annual Review of Biomedical Engineeing 11, 235–257.
Yu, R., Hinkle, P.M., 2000. The Journal of Biological Chemistry 275 (31), 23648–23653.
Zhang, X.L., Yin, H.B., Cooper, J.M., Haswell, S.J., 2006. Electrophoresis 27 (24), 5093–5100.
Zhao, Y.X., Araki, S., Jiahui, W.H., Teramoto, T., Chang, Y.F., Nakano, M., Abdelfattah, A.S., Fujiwara, M., Ishihara, T., Nagai, T., Campbell, R.E., 2011. Science 333 (6051), 1888–1891.